https://doi.org/10.5194/acp-2021-109
Preprint. Discussion started: 22 February 2021

The Effect of Forced and Unforced Variability on Heat Waves, Temperature Extremes, and Associated Population Risk in a CO_2-Warmed World

Jangho Lee, Jeffrey C. Mast, and Andrew E. Dessler

Department of Atmospheric Sciences, Texas A&M University, College Station, TX, USA

Corresponding author: Andrew Dessler (adessler@tamu.edu)

Key Points

- Unforced variability of the climate system, primarily ENSO, plays a key role in the occurrence of extreme events.
- Uncertainty of internal variability is shown to reduce as one looks at larger regions or at a global perspective by using the large Ensembles.
- Increases of heat wave indices are significant between 1.5°C and 2.0°C of warming and the risk of facing extreme heat events is higher in low GDP regions.

https://doi.org/10.5194/acp-2021-109
Preprint. Discussion started: 22 February 2021

Abstract

This study investigates the impact of global warming on heat and humidity extremes by analyzing 6-hourly output from 28 members of the Max Planck Institute Grand Ensemble driven by forcing from a 1%/year CO_2 increase. We find that unforced variability drives large changes in regional exposure to extremes in different ensemble members, and these variations are mostly associated with ENSO variability. However, while the unforced variability of the climate can alter the occurrence of extremes regionally, variability within the ensemble decreases significantly as one looks at larger regions or at a global population perspective. This means that, for metrics of extreme heat and humidity analyzed here, forced variability of the climate is more important than the unforced variability at global scales. Lastly, we found that most heat wave metrics will increase significantly between 1.5°C and 2.0°C, and that low GDP regions shows significant higher risks of facing extreme heat events compared to high GDP regions. Considering the limited economic adaptability of population to heat extremes, this reinforces the idea that the most severe impacts of climate change may fall mostly on those least capable to adapt.

https://doi.org/10.5194/acp-2021-109
Preprint. Discussion started: 22 February 2021

Atmospheric Chemistry and Physics Discussions

1. Introduction

The long-term goal of the 2015 Paris agreement is to keep the increase in global temperature well below 2°C above pre-industrial levels, while pursuing efforts and to limit the warming to 1.5°C. Given that no one lives in the global average, however, understanding how these global average thresholds translate into regional occurrences of extreme heat and humidity is of great value(Harrington et al., 2018). Various studies have reported that regional extreme heat events and heat waves will not only be more frequent, but also more extreme in a warmer world. This was discussed in various assessment and reports such as US National Climate assessment and IPCC (Melillo et al., 2014;Wuebbles et al., 2017;Hoegh-Guldberg et al., 2018;Masson-Delmotte et al., 2018) and it is reported to have significant impacts on human society and health.

Many criteria and indices have been used to assess extreme heat, such as the absolute increase of maximum temperature from the reference period (Wobus et al., 2018), risk ratio (Kharin et al., 2018), and heat wave magnitude index (Russo et al., 2017). In this study, we utilize four locally defined heat wave indices from Fischer and Schär (2010) and Perkins et al. (2012) of duration, frequency, amplitude, and mean. We also focus on consecutive-day extremes, which are known to cause more harm than single-day events (Baldwin et al., 2019;Simolo et al., 2011;Tan et al., 2010). In addition, because the combined effect of temperature and humidity is known to affect human health by reducing the body's ability to cool itself through perspiration, wet-bulb temperature is frequently analyzed (Kang and Eltahir, 2018) and we will do so here.

Climate extremes are always a combination of long-term forced climate change acting in concert with unforced variability (Deser et al., 2012). Thus, characterizing and quantifying the variability of the climate system is crucial in assessing the future risk of extreme events. There

https://doi.org/10.5194/acp-2021-109
Preprint. Discussion started: 22 February 2021

have been numerous studies that links dominant modes of unforced variability to extreme events. Temperature connections with El Niño Southern Oscillation (ENSO) (Thirumalai et al., 2017;Meehl et al., 2007), Pacific Decadal Oscillation (PDO) (Birk et al., 2010) , Atlantic Multidecadal Oscillation (AMO) (Zhang et al., 2020) have been investigated from the previous studies. The effect of climate extremes on different populations depends on the level of economic development, with impacts of heat extremes being more severe in less economically developed countries (Diffenbaugh and Burke, 2019;Harrington et al., 2016;King and Harrington, 2018). For example, as temperatures go up, increased energy demand to cool buildings will be required (Parkes et al., 2019;Sivak, 2009). But this requires resources to both install air conditioning and then run it.

In this paper, a single-model initial-condition ensemble of 28 runs of a global climate model (GCM) is used to quantify heat and humidity extremes in a warmer world. We use population data to look at population risk as well as thresholds for mortality events in daytime (Mora et al., 2017) and nighttime (Chen and Lu, 2014). We also utilize per capita gross domestic product (GDP per capita) data to investigate how climate change impacts different levels of economic status during extreme events. To quantify the impact on energy demand, we also quantify changes in cooling degree days and warming degree days.

The rest of the paper will focus on the following topics: Section 2 describes the model and data used, Section 3 explains the bias-correction method, as well as explaining the metrics used. Section 4 describes the results of the calculations and associated heat wave events in the warmer world as well as the role of unforced variability on extreme heat events. Section 5 summarizes the results and suggests directions for the future work.

https://doi.org/10.5194/acp-2021-109
Preprint. Discussion started: 22 February 2021

2. Data

2.1. MPI-GE ensembles

Simulation data in this study come from an ensemble of runs of the Max-Plank Institute Earth System Model collectively known as the MPI Grand Ensemble (MPI-GE) project (Maher et al., 2019). Each of the 28 ensemble members branches from different points of a 2000-year pre-industrial control run and go for 150 years, forced by CO_2 concentration increasing at 1% per year (hereafter, 1% runs). Because the radiative forcing scales as the log of CO_2 concentration, the 1% runs feature radiative forcing that increases approximately linearly in time. We analyze 6-hourly output with 1.875° × 1.875° spatial resolution for land and near-land ocean areas between 60°N and 60°S. Our analysis will focus on 2-meter temperature (hereafter, t2m) and 2-meter dew point temperature (d2m), from which 2-meter relative humidity and wet-bulb temperature (w2m) are calculated using the equations of Stull (2011).

Unforced variability in the climate system generates uncertainties in the projection of the climate by impacting the dynamic component of the climate, especially for extreme events (Kay et al., 2015;Thompson et al., 2015). In this paper, we use the ensemble to allow us to estimate the impact of unforced variability on temperature extremes.

We also analyze a 100-member ensemble of runs of the same model with historical forcing (hereafter, historical runs), which simulates the years 1850-2005. We also analyze runs with RCP8.5 forcing, which simulate the years 2006-2100. Like the 1% runs, each historical ensemble member and it's RCP 8.5 extension branches from a different point in the same 2000-year control run. This historical and RCP8.5 ensemble only has monthly average fields.

2.2. Global population and GDP per capita data

https://doi.org/10.5194/acp-2021-109
Preprint. Discussion started: 22 February 2021

Global population data from the NASA Socioeconomic Data and Applications Center (SEDAC, 2018) are used to weight the heat wave indices by population. The data represent the population in year 2015 at 30″ × 30″ spatial resolution, and we averaged and re-gridded to the 1.875° × 1.875° grid of the MPI model by summing the values in grid boxes surrounding the MPI grid centers. In our population-weighted calculations, we assume that the relative distribution of population remains fixed into the future.

Gridded GDP per capita data (Kummu, 2019) over 1990-2015 are used to estimate the risk of heat extreme events for different levels of wealth. These data are regridded from the original 5″ × 5″ spatial resolution to the MPI model's resolution of 1.875° × 1.875° by averaging the GDP inside the grid box. When averaging the GDP, per capita GDP has been multiplied by population to estimate the total GDP. Data were then averaged over the 1990-2015 period. We assume that the relative percentile of GDP per capita for each grid point is assumed to be fixed into the future, so changes in climate risk are due to exposure to warmer climate extremes, not changes in relative per capita wealth.

3. Method of analysis

3.1. Global warming

Global warming is defined as the global and annual average temperature increase compared to the first 5 years of the 1% run. We find that ensemble- and global-average t2m reaches 1.5°C, 2°C, and 4°C occur in years 59, 76, and 133 years, respectively, and reaches 4.59°C at the end of the 150-year run. The increase of global average temperature is nearly linear for both t2m and w2m (Figure 1a and 1b), consistent with a linear ramping of the forcing.

https://doi.org/10.5194/acp-2021-109
Preprint. Discussion started: 22 February 2021

3.2. Bias-correction of 1% runs

Many GCMs have systematic biases in surface temperature, and various attempts have been made to correct them (e.g. Li et al. (2010);Thrasher et al. (2012)). In our analysis, we are mainly interested in the spatial pattern of warming, and to judge the fidelity of that in the MPI-ESM 1.1 model, we compare the 1% runs with ERA-Interim reanalysis data (Dee et al., 2011) from European Centre for Medium-range Weather Forecast (ECMWF). To do this, we compared the period 2003-2017 in the ERA-interim with a 15-year period in the 1% runs (years 39-53) with the same ensemble- and global-average absolute temperature. The ensemble and area-averaged bias for land and near-land ocean areas archived in the 6-hourly dataset is near zero for t2m, but underestimates w2m over this period by 0.18°C (Figure 1).

But while the ensemble- and area-averaged t2m bias is near zero, the difference is not zero at all grid points of individual ensemble members. Figures 2a and 2b show the difference in the 90th percentile value of t2m and w2m at each grid point calculated over the 15-year period in the model ensemble minus the 90th percentile value at the same grid point in the ERA-Interim. Figures 2c and 2d show the difference in median values.

This bias is not the result of unforced variability — it is consistent in all ensemble members. To show this, we calculate at each grid point the difference between the highest and lowest 90th percentile temperature in the ensemble divided by the ensemble average 90th percentile temperature bias between reanalysis data the ensemble, computed where the bias is greater than 2°C (Figure 2e). We also do the same for the median temperature (Figure 2f). The disagreement between the ensembles is at most 37% of the bias in the same region, and the average is 13% (Figures 2e, f). In other words, the systematic bias of the model compared to reanalysis exceeds the spread within the ensemble.

https://doi.org/10.5194/acp-2021-109
Preprint. Discussion started: 22 February 2021

Atmospheric Chemistry and Physics Discussions

The CDF-t method (Michelangeli et al., 2009) is used to bias correct each ensemble member of the 1% runs. CDF-t method finds the transformation function that maps the cumulative density function (CDF) of a GCM to the CDF of a historical reanalysis data in a reference period, which is year 39-53 in 1% runs and 2003-2017 for ERA-Interim reanalysis data. This function is then applied to the 1% runs to generate bias-corrected fields. For the values that fall outside the limits of the CDFs in the reference period, linear extrapolation is used. CDF-t is known to realistically correct the temperature and precipitation output of GCMs, especially for extreme events (Vrac et al., 2012;Watanabe et al., 2012).

Bias correction via CDF-t is done for t2m and d2m, and then rh and w2m are calculated with these bias-corrected fields. The bias is reduced significantly for all regions for both t2m and w2m (Figures 1c, 1d, 2a-2d). The bias in w2m is mostly caused by the small remaining biases in t2m and d2m, which are amplified in the w2m calculation. Hereafter, '1% runs' will refer to the bias-corrected 1% runs.

Since the 1% runs are CO_2-only forcing, without aerosol forcing, one might wonder whether the temperature extremes estimated by these models would apply to a world with a more realistic forcing that includes aerosols. To determine this, we have compared monthly average and monthly maximum temperatures from an ensemble of 100 RCP 8.5 scenario runs from the MPI-GE to the same quantities estimated from the 1% ensemble. If we compare the ensembles at points in time when they have 1.5, 2, 3, and 4°C of ensemble- and global-average warming, we find very small regional differences — the regional ensemble averaged maximum and mean temperature difference was less than 0.5°C in all regions. Alternatively, since we bias-corrected the 1% CO_2 runs to reanalysis data, which contains aerosol forcing, our bias-corrected 1% CO_2

https://doi.org/10.5194/acp-2021-109
Preprint. Discussion started: 22 February 2021

Atmospheric Chemistry and Physics Discussions

runs can be understood as a continuously warming climate driven by CO_2, with effect of aerosols fixed at 2003-2017 period.

3.3. Heat wave indices

Identification of heat waves is done in several steps. First, we smooth a daily maximum temperature (determined form 6-hourly temperatures) using a 15-day moving window for the first 5 years of 1% runs, which is the period before significant warming has occurred. This was done at each grid points, followed by a framework from Fischer and Schär (2010). Then, also for each grid point, the 90th percentile of smoothed daily maximum temperature for the first 5 years was calculated. This value is used as a threshold for the heat waves. After calculating the threshold, we calculate the heat wave days, defined as days that exceeds the threshold for three or more consecutive days (Baldwin et al., 2019).

We then define four indices to represent the characteristics of these heat waves. To determine the occurrence of events, heat wave duration (HWD; longest heat wave of the year) and heat wave frequency (HWF; total number of heat wave days in a year) are calculated. From an intensity perspective, heat wave amplitude (HWA; maximum temperature during heat wave days during a year) and heat wave mean (HWM; mean temperature during heat wave days in a year) are selected. These indices are also calculated in an analogous fashion for wet bulb temperature (w2m), since wet-bulb temperature is arguably more relevant for human health (Heo et al., 2019;Morris et al., 2019;Buzan and Huber, 2020). These indices are summarized in Table 1.

3.4. Deadly days and tropical nights

https://doi.org/10.5194/acp-2021-109
Preprint. Discussion started: 22 February 2021

Heat wave thresholds are different for each grid point because they are based on pre-industrial baseline at that grid point. Combined with regional differences in the ability to adapt, this means that heat waves in different regions may have different implications for human society. We therefore also count the number of days each year with w2m above 24°C, which we refer to as “deadly days”. This value is consistent with the analysis of Mora et al. (2017), who demonstrated that this is the threshold above which fatalities from heat-related illness occur. A warm nighttime minimum temperature can be as important as a high maximum temperature for human health and mortality (Argaud et al., 2007;Patz et al., 2005), so we define “tropical nights” as a daily minimum t2m over 25°C (Lelieveld et al., 2012).

3.5. Cooling degree days and heating degree days

To assess the economic and energy impact of heat extremes, cooling degree days (CDD) and heating degree days (HDD) are calculated. CDD and HDD are metrics of the energy demand to cool and heat buildings. For each grid point, annual CDD is calculated by subtracting 18°C from the daily average temperature and summing only the positive values over the year. HDD is the absolute value of the sum of the negative values. Although energy demand could be highly linked to the culture, wealth, population of the region and other meteorological conditions rather than the daily mean temperature, previous studies reported that CDD and HDD are closely related to energy consumption (Sailor and Muñoz, 1997).

4. Results

4.1. Impact of unforced variability of climate on regional heat extremes

https://doi.org/10.5194/acp-2021-109
Preprint. Discussion started: 22 February 2021

Atmospheric Chemistry and Physics Discussions

To investigate the impact of unforced variability on more regional heat extremes, we select 15 large cities spread around the world (Fig. 3a). Figure 3b-d shows the maximum spread in the number of deadly days and tropical nights within the ensemble — i.e., the difference between the ensemble member with the highest values of extreme events (deadly days, tropical nights) minus the member with the lowest — at a year when ensemble- and global-average temperature reaches the threshold.

This difference within the ensemble is the result of unforced variability and we see that it varies considerably among the cities. For example, Moscow shows a small spread within the ensemble members for both deadly days and tropical nights for all periods of global warming. This is because, even with 4°C of warming, Moscow experiences a maximum of only 8 deadly days and 25 tropical nights per year. In contrast, with 3°C of warming, a warmer city such as Kinshasa experiences 148 more deadly days in some ensembles than others, and 55 more tropical nights. For all 15 cities, average spread in the number of deadly days at 1.5°C, 2.0°C, 3.0°C , and 4.0°C of global warming between the ensemble members with maximum and minimum numbers is 53.5, 53.2, 63.6, and 56.8 days per year. For tropical nights, the spread is 50.4, 50.3, 50.9, and 52.2 days per year. So, on average, unforced variability can change the number of extreme days and nights by about two months per year.

Previous work has attempted to distinguish the origin and mechanisms of unforced variability from temperature and temperature extremes (Meehl et al., 2007;Zhang et al., 2020;Birk et al., 2010). To probe the physical mechanisms affecting this spread of ensembles, empirical orthogonal function (EOF) analysis was performed separately on the detrended and normalized time series of deadly days and tropical nights for the 15 cities across the ensemble.

https://doi.org/10.5194/acp-2021-109
Preprint. Discussion started: 22 February 2021

We aim to find the dominant drivers of unforced variability that impacts representative cities around the world.

The first three EOF patterns are plotted in Fig. 4. The first EOF mode of deadly days per year in 15 cities show similar signs for all cities except Istanbul and Kinshasa, where the magnitude of the EOF is small for both cities. This means that, if one of the cities is hot, then the others also tend to be hot. The second and third EOFs for deadly days shows more variability between the cities. The EOFs for tropical nights (Fig. 4d, 4e, 4f) shows more variability, with higher number of tropical nights in some cities associated with lower values in others.

The PC time series are projected onto detrended annual sea surface temperature (SST) anomalies. This allows us to investigate how heat extreme events in 15 major cities are associated with global modes of internal variability. This is also plotted in Fig. 4. All of the projections of deadly day PCs and projections of the first two modes of tropical nights shows patterns similar to El Niño-Southern Oscillation (ENSO) and Pacific Decadal Oscillation (PDO). Characteristic patterns for ENSO, PDO, and AMO are calculated for each ensemble using all 150-year of SSTs, and the pattern is averaged over ensembles to come up with a single ENSO, PDO, and AMO SST for the ensemble. Then, those patterns are compared with the PC projection on SST. Correlation coefficients between the standard climate indices and PC projected SST is shown on lower panel of Fig. 4.

Power spectra of the PCs are plotted in Figure 5. Overall, the spectra of the deadly day PCs look very much like the spectrum for ENSO, but does not have the ~20-year peak of the PDO spectrum. This tells us that, in this model at least, the variability in the occurrence of deadly days in these large cities is strongly regulated by ENSO. The third deadly day PC has lower correlations with ENSO or PDO index and a peak at both the ENSO period a slightly

https://doi.org/10.5194/acp-2021-109
Preprint. Discussion started: 22 February 2021

longer period than ENSO, about 10 years, so it is harder to draw firm conclusions about the mechanism behind it.

The tropical night PCs also show peaks at ENSO periods (Fig. 5b) suggesting that, like deadly days, tropical night variability is controlled by ENSO. However, the PC-projected SST of the third EOF of tropical nights shows high values near Northern Africa and East Asian region, suggesting that this EOF represents the effect of ENSO on tropical night variability in this region.

4.2. Cluster analysis and population risk of heat wave indices

We calculate HWD, HWF, HWA, and HWM for both t2m and w2m each year at each grid point, which generates eight different 150-year time series for each of the 28 ensemble members. Each time series at each grid point is regressed vs. time, yielding a slope and the intercept for each time series in all of the 28 ensemble members. The 16 variables (8 [heat wave indices] × 2 [slope, intercept]) are then utilized as a predictor variable for K-means clustering (Likas et al., 2003) to categorize the spatial variation of heat waves. K-means clustering aims to classify the observations (grid point over land) into clusters using the Euclidean distance of its predictor variables (16 variables). The number of clusters (K) in this study is set to 6, using the elbow method (Syakur et al., 2018).

Figure 6a shows the cluster value that most ensembles assigned to each grid point and it shows distinct geographical characteristics, as summarized in Table 2 (the result of clustering shows little difference between the ensemble members). As might be expected, each cluster shows a different evolution of heat extremes in warmer world (Figure 7). Although the warming signal is largest in the polar regions (Figure 6b), the largest increases of HWD and HWF are

https://doi.org/10.5194/acp-2021-109
Preprint. Discussion started: 22 February 2021

observed at lower latitudes (in cluster 1 and 2 on Figure 7a-d). This is due to low variability in these regions compared to polar regions, making it easier for a trend to exceed the heatwave threshold.

For HWA and HWM, the rate of increase is similar for all clusters, with increases of HWA_{t2m} and HWA_{w2m} of 3.5 and 2.2°C, respectively (Figure 7e-h). The exception is HWA_{t2m} in cluster 6. The large increase of HWA_{t2m} in this region is connected to the strong global warming signal in high latitudes that has been predicted for decades and now observed (Stouffer and Manabe, 2017).

Turning to deadly days (Fig. 7i), we find a substantial increase occurs in cluster 1 after 1.5°C of warming; this is important because it gives additional support for the Paris Agreement's aspirational goal of limiting global warming to 1.5°C. Almost all of the increases in deadly days are in low latitudes (cluster 1, 2, and 3). For tropical nights, low latitudes as well as deserts (cluster 4) contribute most of the increase. These regions also show more rapid increases when global average warming exceeds 1.5-2°C.

Figure 7 also shows the spread in within the ensemble for each metric and cluster. We find that the spread for a cluster is generally smaller than the differences between the clusters. This suggests that the differences obtained are not due to interannual variability.

We also generated indices weighted by population. Heat wave indices for the 90th percentile of population (meaning 10% of the population is exposed to higher values) and median of the population are depicted in Figure 8. Figure 8a shows that with 4°C of warming, 10% of the Earth's population will experience heat waves lasting 131 days, and half of the population will experience heat waves around 64 days long. These are large increases over present-day values of 35 days and 17 days. Notably, the average of the standard deviation

https://doi.org/10.5194/acp-2021-109
Preprint. Discussion started: 22 February 2021

Atmospheric Chemistry and Physics Discussions

between the ensembles during 150-yr period are 6.7 days and 3.4 days for the 90th percentile and median, respectively. This is significantly smaller than values from the regional analyses of cities in Figure 3, where the unforced variability can make a huge difference in the occurrence of heat waves.

The rate of increase of HWD_{w2m} and HWF_{w2m} in Fig. 8 accelerates when global average warming exceeds 1-1.5°C. Given that the planet has already warmed about 1°C above pre-industrial, this suggests that the world may be on the cusp of a rapid increase in wet-bulb extremes. This is related to the increased slope in Figure 7, in which cluster 1 and 2's values of HWD_{w2m} and HWF_{w2m} increase rapidly between 1.5C and 2.5°C of global warming. At warmer temperatures, HWD_{w2m} and HWF_{w2m} reach a plateau, since values over 300 days per year means there is little room for additional increase. For $HWA_{t2m/w2m}$ and $HWM_{t2m/w2m}$, the increase is mostly linear. Also note that at 4°C of global warming, HWA_{w2m} reaches 30°C, which while not immediately fatal to humans may nevertheless indicate great difficulty for even a developed society to adapt to.

Currently, 5% of the total population faces more than 180 deadly days and 302 tropical nights per year. This grows to 204 and 333 days, respectively, at 1.5°C warming. With 2°C of global warming, half of the population will face 2 months of deadly days every year and with 2.5°C of global warming, and 5% of the population will be in an environment where every day in a year is a tropical night. With 2°C of global warming, the minimum ensemble member of deadly days and tropical nights is above the maximum ensemble of the current climate. Further details are also shown in Table 3.

It is notable that, although there is a large spread between the ensemble members in each city (Figure 3), the spread in the clusters (Figure 7) and population-weighted metrics (Figure 8)

https://doi.org/10.5194/acp-2021-109
Preprint. Discussion started: 22 February 2021

Atmospheric Chemistry and Physics Discussions

is not as large. This emphasizes that the effect of unforced variability might be large in small regions, but as the region expands, opposite signs of variability cancel, so area-average variability decreases. This is also found in Table 3, where in each case, the standard deviation between ensembles is less than 10% of the average. This indicates that internal variability will play a minor role in determining global exposure to temperature thresholds, although different people may be affected in different climate realizations.

In addition, with 1.5°C of global warming, the lowest ensemble of the 90th percentile of HWD_{t2m}, HWD_{w2m}, and HWF_{t2m} exceeds the highest ensemble of the same metric in the current climate (red lines in Figure 8). With 2°C of warming, the minimum ensemble of HWF_{w2m}, HWA_{t2m}, HWA_{w2m}, and HWM_{w2m} exceed the maximum ensemble of the current climate, and with 2.5°C of warming, the minimum ensemble of all metrics exceeds the maximum ensemble of the same metric in the current climate. Thus, this model predicts that the occurrence of extremes will soon be able to exceed values likely possible in our present climate.

4.3. Analysis on GDP per capita

It is well-known that not everyone is equally vulnerable to extreme weather, with rich, developed countries having more resources to deal with extreme events. In that context, global gridded GDP per capita is used to calculate average risk at each level of wealth. The ensemble-average result is depicted in Figure 9, which shows the increased number of deadly days and tropical nights that each level of economic level experience relative to today's current level of global warming. This plot assumes that the distribution of population and GDP remains fixed through time.

https://doi.org/10.5194/acp-2021-109
Preprint. Discussion started: 22 February 2021

With 0.5°C increase of global warming, population in lowest 10% of GDP will face 28 more deadly days and 22 more tropical nights increasing compared to present day. In contrast, the richest 10% will experience 5 and 3 more deadly days and tropical nights for the same warming. At 3°C above current temperatures (about 4°C above preindustrial temperatures), the population with the lowest 10% of GDP will experience154 and 162 more days of deadly days and tropical nights compared to today's climate. On the other hand, population with the highest 10% of GDP will experience an increase of 26 and 30 days for the same warming. The regions that contribute the most for the low GDP percentiles are Tropical Africa, including Republic of the Congo, Kenya, Uganda, Ethiopia, and Sudan, which are in clusters 1 and 2 in our cluster analysis. The maximum difference of heat wave days between the ensembles is less than 25% for all GDP and global warming levels.

4.4. Energy demand on large cities

Annual CDD and HDD have been calculated for the 15 cities in section 4.1. Fig. 10 shows the percent change of CDD and HDD at 1.5°C, 2.0°C, 3.0°C, and 4.0°C relative to the pre-industrial CDD and HDD values (average of first 5 year of 1% CO_2 runs). This was done for each city, and for each ensemble member. In 1.5°C, 2.0°C, 3.0°C, and 4.0°C warming, CDD in 15 cities increases by 26%, 38%, 60%, and 82%. This suggests an enormous increase in energy required for cooling. In contrast, energy demand on cold days (HDD) decreases by 51%, 60%, 68%, and 75%, compared to pre-industrial baseline, suggesting a partially offsetting decrease in energy required for heating. The spread between the ensemble members is small compared to the average of the ensembles, except for Moscow.

https://doi.org/10.5194/acp-2021-109
Preprint. Discussion started: 22 February 2021

Atmospheric Chemistry and Physics Discussions

Large percentage increases in CDD for Moscow is the result of low pre-industrial CDD values, so that (relatively) small increases in CDD correspond to large fractional changes, as well as large differences between ensemble members. The ensemble spread of HDD in Moscow is also large, compared to other cities. This is not due to low values of HDD – Moscow has highest HDD value among 15 cities (4062 days °C per year in pre-industrial condition) — but rather that unforced variability of the climate is more important for HDD than CDD values for Moscow.

5. Conclusion

In this study, we found that extreme heat events will become more frequent and severe in a continuously warming world. In a warmer world, duration, frequency, amplitude, and mean of extreme heat and humidity events increase, especially in low-latitude regions. In some of the regions, wet bulb temperature will reach upper 20s, which is above the level that significantly impact human mortality. We also find and quantify the impact of forced change and unforced variability on the extreme heat events.

Our results show that ENSO is the dominant mode of unforced variability impacting the occurrence of extreme heat and humidity events and that events tend to be synchronous in 15 large cities we chose. But while the impact of unforced variability might be significant regionally, it narrows down when one looks at larger aggregate regions.

Looking at the population-weighted stats, we found that with 1.5°C of global average warming, over 10% of population will face heat waves of 42°C temperature, and 27°C wet bulb temperatures. With 4°C warming, 10% of population will face 45°C temperature and 29°C wet bulb temperature. Also, even with 1.5°C of warming, which is about 0.5°C higher than the current level, 5% of the population will face more than 200 days of deadly days and over 300

https://doi.org/10.5194/acp-2021-109
Preprint. Discussion started: 22 February 2021

Atmospheric Chemistry and Physics Discussions

days of tropical nights per year. With 4°C of warming, 10% of the population will experience over 300 days of deadly days and over 330 days of tropical nights per year. Given these two metrics are based on human mortality, this may have significant impact on human health globally.

Sorting heat and humidity events by wealth, we found that increasing frequency and severity of extreme events will fall mostly on the poorest people. Given underdeveloped countries' lack of ability to endure climate extremes, and that they have contributed the least to climate change, this introduces a profound moral dimension to the problem. To further investigate the economic impacts of increasing heat extremes, cooling degree days (CDD) and heating degree days (HDD) are calculated for 15 large cities. Energy demand for cooling (CDD) increases by average of 26% on 1.5°C and 82% on 4.0°C of warming, while energy demand for heating (HDD) decreases by 51% and 75%. Since CDD is known to have a conditionally linear relationship with the energy consumption, with slope increasing with higher CDD (De Rosa et al., 2014;Shin and Do, 2016), increasing CDD in a warmer world could be one of the factors driving increased economic inequity from global warming related heat extremes, due to high cost and demand for energy in poorest countries.

Uncertainties in this analysis include our use of gridded 6-hourly climate model output. Another uncertainty is that our runs are continuously warming, and it is possible that an equilibrium world at any given temperature may experience different occurrence of extremes than in the runs in this paper. Additionally, since an increasing proportion of the population lives in dense metropolitan areas, there is also the possibility that actual heat and humidity extremes that populations experience could be more severe than the gridded data due to local phenomena such as the urban heat island effect (Murata et al., 2012). Statistical or dynamical downscaling

https://doi.org/10.5194/acp-2021-109
Preprint. Discussion started: 22 February 2021

Atmospheric Chemistry and Physics Discussions

could be used for a more detailed analysis (Dibike and Coulibaly, 2006;Wood et al., 2004). This was not done in this study because the model we used is already bias-corrected, so another downscaling would affect the consistency of the model. However, better understanding and evaluation of the actual temperatures people are projected to experience would be a useful next step.

Author contribution

Conceptualization: J.L., J.M, and A.D. Data curation: J.L. and A.D. Formal analysis: J.L. and J.M. Funding acquisition: A.D. Investigation: J.L. and J.M. Methodology: J.L. Project administration: A.D. Resources: A.D. Software: J.L. Supervision: A.D. Visualization: J.L. Writing: J.L. and A.D.

Competing interests

The authors declare that they have no conflict of interest.

Acknowledgments

This work was supported by NSF grants AGS-1661861 and AGS-1841308, both to Texas A&M University. The authors declare that there is no conflict of interest regarding the publication of this article.

https://doi.org/10.5194/acp-2021-109
Preprint. Discussion started: 22 February 2021

Atmospheric Chemistry and Physics
Discussions

References

Argaud, L., Ferry, T., Le, Q. H., Marfisi, A., Ciorba, D., Achache, P., Ducluzeau, R., and Robert, D.: Short- and long-term outcomes of heatstroke following the 2003 heat wave in Lyon, France, Archives of Internal Medicine, 167, 2177-2183, DOI 10.1001/archinte.167.20.ioi70147, 2007.

Baldwin, J. W., Dessy, J. B., Vecchi, G. A., and Oppenheimer, M.: Temporally Compound Heat Wave Events and Global Warming: An Emerging Hazard, Earths Future, 7, 411-427, 10.1029/2018ef000989, 2019.

Birk, K., Lupo, A. R., Guinan, P., and Barbieri, C.: The interannual variability of midwestern temperatures and precipitation as related to the ENSO and PDO, Atmosfera, 23, 95-128, 2010.

Buzan, J. R., and Huber, M.: Moist heat stress on a hotter Earth, Annual Review of Earth and Planetary Sciences, 48, 2020.

Chen, R. D., and Lu, R. Y.: Dry Tropical Nights and Wet Extreme Heat in Beijing: Atypical Configurations between High Temperature and Humidity, Monthly Weather Review, 142, 1792-1802, 10.1175/Mwr-D-13-00289.1, 2014.

De Rosa, M., Bianco, V., Scarpa, F., and Tagliafico, L. A.: Heating and cooling building energy demand evaluation; a simplified model and a modified degree days approach, Applied energy, 128, 217-229, 2014.

Dee, D. P., Uppala, S. M., Simmons, A. J., Berrisford, P., Poli, P., Kobayashi, S., Andrae, U., Balmaseda, M. A., Balsamo, G., Bauer, P., Bechtold, P., Beljaars, A. C. M., van de Berg, L., Bidlot, J., Bormann, N., Delsol, C., Dragani, R., Fuentes, M., Geer, A. J., Haimberger, L., Healy, S. B., Hersbach, H., Holm, E. V., Isaksen, L., Kallberg, P., Kohler, M., Matricardi, M., McNally, A. P., Monge-Sanz, B. M., Morcrette, J. J., Park, B. K., Peubey, C., de Rosnay, P., Tavolato, C., Thepaut, J. N., and Vitart, F.: The ERA-Interim reanalysis: configuration and performance of the data assimilation system, Quarterly Journal of the Royal Meteorological Society, 137, 553-597, 10.1002/qj.828, 2011.

Deser, C., Phillips, A., Bourdette, V., and Teng, H. Y.: Uncertainty in climate change projections: the role of internal variability, Climate Dynamics, 38, 527-546, 10.1007/s00382-010-0977-x, 2012.

Dibike, Y. B., and Coulibaly, P.: Temporal neural networks for downscaling climate variability and extremes, Neural Networks, 19, 135-144, 10.1016/j.neunet.2006.01.003, 2006.

Diffenbaugh, N. S., and Burke, M.: Global warming has increased global economic inequality, Proceedings of the National Academy of Sciences, 116, 9808-9813, 2019.

Fischer, E. M., and Schär, C.: Consistent geographical patterns of changes in high-impact European heatwaves, Nature Geoscience, 3, 398-403, 2010.

Harrington, L. J., Frame, D. J., Fischer, E. M., Hawkins, E., Joshi, M., and Jones, C. D.: Poorest countries experience earlier anthropogenic emergence of daily temperature extremes, Environmental Research Letters, 11, 055007, 2016.

Harrington, L. J., Frame, D., King, A. D., and Otto, F. E.: How uneven are changes to impact-relevant climate hazards in a 1.5° C world and beyond?, Geophysical Research Letters, 45, 6672-6680, 2018.

Heo, S., Bell, M. L., and Lee, J. T.: Comparison of health risks by heat wave definition: Applicability of wet-bulb globe temperature for heat wave criteria, Environmental Research, 168, 158-170, 10.1016/j.envres.2018.09.032, 2019.

https://doi.org/10.5194/acp-2021-109
Preprint. Discussion started: 22 February 2021

Atmospheric Chemistry and Physics Discussions

Hoegh-Guldberg, O., Jacob, D., Bindi, M., Brown, S., Camilloni, I., Diedhiou, A., Djalante, R., Ebi, K., Engelbrecht, F., and Guiot, J.: Impacts of 1.5 C global warming on natural and human systems, Global warming of 1.5° C. An IPCC Special Report, 2018.

Kang, S., and Eltahir, E. A. B.: North China Plain threatened by deadly heatwaves due to climate change and irrigation, Nat Commun, 9, 2894, 10.1038/s41467-018-05252-y, 2018.

Kay, J. E., Deser, C., Phillips, A., Mai, A., Hannay, C., Strand, G., Arblaster, J. M., Bates, S. C., Danabasoglu, G., Edwards, J., Holland, M., Kushner, P., Lamarque, J. F., Lawrence, D., Lindsay, K., Middleton, A., Munoz, E., Neale, R., Oleson, K., Polvani, L., and Vertenstein, M.: THE COMMUNITY EARTH SYSTEM MODEL (CESM) LARGE ENSEMBLE PROJECT A Community Resource for Studying Climate Change in the Presence of Internal Climate Variability, Bulletin of the American Meteorological Society, 96, 1333-1349, 10.1175/Bams-D-13-00255.1, 2015.

Kharin, V. V., Flato, G. M., Zhang, X., Gillett, N. P., Zwiers, F., and Anderson, K. J.: Risks from Climate Extremes Change Differently from 1.5 degrees C to 2.0 degrees C Depending on Rarity, Earths Future, 6, 704-715, 10.1002/2018ef000813, 2018.

King, A. D., and Harrington, L. J.: The inequality of climate change from 1.5 to 2 C of global warming, Geophysical Research Letters, 45, 5030-5033, 2018.

Kummu, M. T., Maija; Guillaume, Joseph H. A.: Data from: Gridded global datasets for Gross Domestic Product and Human Development Index over 1990-2015 Dryad, Dataset, https://doi.org/10.5061/dryad.dk1j0. 2019.

Lelieveld, J., Hadjinicolaou, P., Kostopoulou, E., Chenoweth, J., El Maayar, M., Giannakopoulos, C., Hannides, C., Lange, M. A., Tanarhte, M., Tyrlis, E., and Xoplaki, E.: Climate change and impacts in the Eastern Mediterranean and the Middle East, Climatic Change, 114, 667-687, 10.1007/s10584-012-0418-4, 2012.

Li, H. B., Sheffield, J., and Wood, E. F.: Bias correction of monthly precipitation and temperature fields from Intergovernmental Panel on Climate Change AR4 models using equidistant quantile matching, Journal of Geophysical Research-Atmospheres, 115, Artn D10101 10.1029/2009jd012882, 2010.

Likas, A., Vlassis, N., and Verbeek, J. J.: The global k-means clustering algorithm, Pattern Recognition, 36, 451-461, 2003.

Maher, N., Milinski, S., Suarez-Gutierrez, L., Botzet, M., Dobrynin, M., Kornblueh, L., Kroger, J., Takano, Y., Ghosh, R., Hedemann, C., Li, C., Li, H. M., Manzini, E., Notz, D., Putrasahan, D., Boysen, L., Claussen, M., Ilyina, T., Olonscheck, D., Raddatz, T., Stevens, B., and Marotzke, J.: The Max Planck Institute Grand Ensemble: Enabling the Exploration of Climate System Variability, Journal of Advances in Modeling Earth Systems, 11, 2050-2069, 10.1029/2019ms001639, 2019.

Masson-Delmotte, V., Zhai, P., Pörtner, H.-O., Roberts, D., Skea, J., Shukla, P. R., Pirani, A., Moufouma-Okia, W., Péan, C., and Pidcock, R.: Global warming of 1.5 C, An IPCC Special Report on the impacts of global warming of, 1, 2018.

Meehl, G. A., Tebaldi, C., Teng, H., and Peterson, T. C.: Current and future US weather extremes and El Niño, Geophysical Research Letters, 34, 2007.

Melillo, J. M., Richmond, T., and Yohe, G.: Climate change impacts in the United States, Third national climate assessment, 52, 2014.

Michelangeli, P. A., Vrac, M., and Loukos, H.: Probabilistic downscaling approaches: Application to wind cumulative distribution functions, Geophysical Research Letters, 36, Artn L11708

https://doi.org/10.5194/acp-2021-109
Preprint. Discussion started: 22 February 2021

Atmospheric Chemistry and Physics Discussions

10.1029/2009gl038401, 2009.

Mora, C., Dousset, B., Caldwell, I. R., Powell, F. E., Geronimo, R. C., Bielecki, C. R., Counsell, C. W., Dietrich, B. S., Johnston, E. T., Louis, L. V., Lucas, M. P., McKenzie, M. M., Shea, A. G., Tseng, H., Giambelluca, T., Leon, L. R., Hawkins, E., and Trauernicht, C.: Global risk of deadly heat, Nature Climate Change, 7, 501-+, 10.1038/Nclimate3322, 2017.

Morris, C. E., Gonzales, R. G., Hodgson, M. J., and Tustin, A. W.: Actual and simulated weather data to evaluate wet bulb globe temperature and heat index as alerts for occupational heat-related illness, Journal of Occupational and Environmental Hygiene, 16, 54-65, 10.1080/15459624.2018.1532574, 2019.

Murata, A., Nakano, M., Kanada, S., Kurihara, K., and Sasaki, H.: Summertime temperature extremes over Japan in the late 21st century projected by a high-resolution regional climate model, Journal of the Meteorological Society of Japan. Ser. II, 90, 101-122, 2012.

Parkes, B., Cronin, J., Dessens, O., and Sultan, B.: Climate change in Africa: costs of mitigating heat stress, Climatic Change, 154, 461-476, 2019.

Patz, J. A., Campbell-Lendrum, D., Holloway, T., and Foley, J. A.: Impact of regional climate change on human health, Nature, 438, 310-317, 10.1038/nature04188, 2005.

Perkins, S., Alexander, L., and Nairn, J.: Increasing frequency, intensity and duration of observed global heatwaves and warm spells, Geophysical Research Letters, 39, 2012.

Russo, S., Sillmann, J., and Sterl, A.: Humid heat waves at different warming levels, Scientific Reports, 7, ARTN 7477

10.1038/s41598-017-07536-7, 2017.

Sailor, D. J., and Muñoz, J. R.: Sensitivity of electricity and natural gas consumption to climate in the USA—Methodology and results for eight states, Energy, 22, 987-998, 1997.

SEDAC: Gridded Population of the World, Version 4 (GPWv4): Population Density, Revision 11. Palisades, NY: NASA 2018.

Shin, M., and Do, S. L.: Prediction of cooling energy use in buildings using an enthalpy-based cooling degree days method in a hot and humid climate, Energy and Buildings, 110, 57-70, 2016.

Simolo, C., Brunetti, M., Maugeri, M., and Nanni, T.: Evolution of extreme temperatures in a warming climate, Geophysical Research Letters, 38, Artn L16701

10.1029/2011gl048437, 2011.

Sivak, M.: Potential energy demand for cooling in the 50 largest metropolitan areas of the world: Implications for developing countries, Energy Policy, 37, 1382-1384, 2009.

Stouffer, R. J., and Manabe, S.: Assessing temperature pattern projections made in 1989, Nature Climate Change, 7, 163-165, 2017.

Stull, R.: Wet-Bulb Temperature from Relative Humidity and Air Temperature, Journal of Applied Meteorology and Climatology, 50, 2267-2269, 10.1175/Jamc-D-11-0143.1, 2011.

Syakur, M. A., Khotimah, B. K., Rochman, E. M. S., and Satoto, B. D.: Integration K-Means Clustering Method and Elbow Method For Identification of The Best Customer Profile Cluster, 2nd International Conference on Vocational Education and Electrical Engineering (Icvee), 336, Unsp 012017

10.1088/1757-899x/336/1/012017, 2018.

https://doi.org/10.5194/acp-2021-109
Preprint. Discussion started: 22 February 2021

Atmospheric Chemistry and Physics Discussions

Tan, J. G., Zheng, Y. F., Tang, X., Guo, C. Y., Li, L. P., Song, G. X., Zhen, X. R., Yuan, D., Kalkstein, A. J., Li, F. R., and Chen, H.: The urban heat island and its impact on heat waves and human health in Shanghai, International Journal of Biometeorology, 54, 75-84, 10.1007/s00484-009-0256-x, 2010.

Thirumalai, K., DiNezio, P. N., Okumura, Y., and Deser, C.: Extreme temperatures in Southeast Asia caused by El Nino and worsened by global warming, Nat Commun, 8, 15531, 10.1038/ncomms15531, 2017.

Thompson, D. W. J., Barnes, E. A., Deser, C., Foust, W. E., and Phillips, A. S.: Quantifying the Role of Internal Climate Variability in Future Climate Trends, Journal of Climate, 28, 6443-6456, 10.1175/Jcli-D-14-00830.1, 2015.

Thrasher, B., Maurer, E. P., McKellar, C., and Duffy, P. B.: Technical Note: Bias correcting climate model simulated daily temperature extremes with quantile mapping, Hydrology and Earth System Sciences, 16, 3309-3314, 10.5194/hess-16-3309-2012, 2012.

Vrac, M., Drobinski, P., Merlo, A., Herrmann, M., Lavaysse, C., Li, L., and Somot, S.: Dynamical and statistical downscaling of the French Mediterranean climate: uncertainty assessment, Natural Hazards and Earth System Sciences, 12, 2769-2784, 10.5194/nhess-12-2769-2012, 2012.

Watanabe, S., Kanae, S., Seto, S., Yeh, P. J. F., Hirabayashi, Y., and Oki, T.: Intercomparison of bias-correction methods for monthly temperature and precipitation simulated by multiple climate models, Journal of Geophysical Research-Atmospheres, 117, Artn D23114

10.1029/2012jd018192, 2012.

Wobus, C., Zarakas, C., Malek, P., Sanderson, B., Crimmins, A., Kolian, M., Sarofim, M., and Weaver, C. P.: Reframing Future Risks of Extreme Heat in the United States, Earths Future, 6, 1323-1335, 10.1029/2018ef000943, 2018.

Wood, A. W., Leung, L. R., Sridhar, V., and Lettenmaier, D. P.: Hydrologic implications of dynamical and statistical approaches to downscaling climate model outputs, Climatic Change, 62, 189-216, DOI 10.1023/B:CLIM.0000013685.99609.9e, 2004.

Wuebbles, D. J., Fahey, D. W., and Hibbard, K. A.: Climate science special report: fourth national climate assessment, volume I, 2017.

Zhang, G., Zeng, G., Li, C., and Yang, X.: Impact of PDO and AMO on interdecadal variability in extreme high temperatures in North China over the most recent 40-year period, Climate Dynamics, 54, 3003-3020, 2020.

https://doi.org/10.5194/acp-2021-109
Preprint. Discussion started: 22 February 2021

Atmospheric Chemistry and Physics
Open Access
Discussions

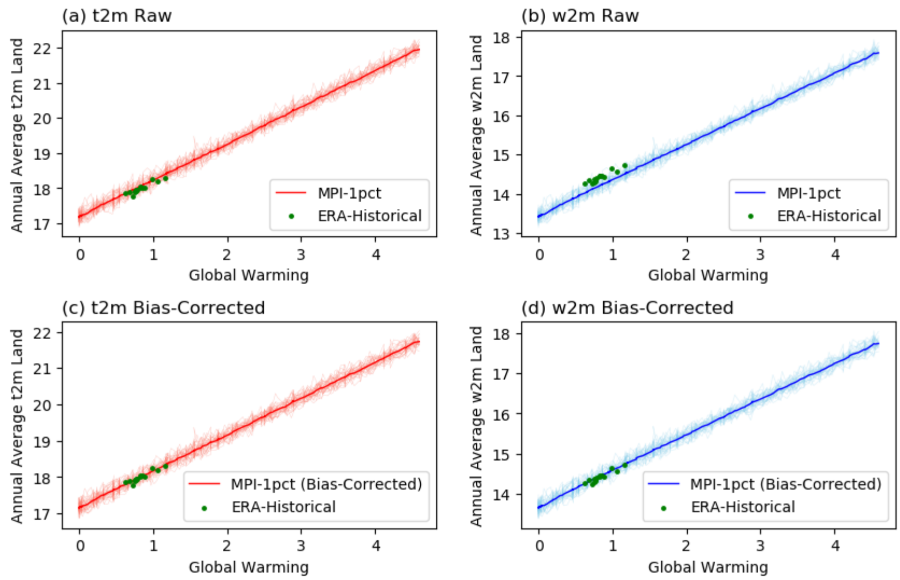

Figure 1. (a) Annual average temperature (t2m) for 150-yr 1% runs, calculated for land and near-land ocean areas. Green dots show the historical record of ERA-Interim for the corresponding global warming levels. (b) Same as (a), but for wet-bulb temperature (w2m). (c, d) same as (a, b), but for the bias-corrected 1% runs.

https://doi.org/10.5194/acp-2021-109
Preprint. Discussion started: 22 February 2021

Atmospheric Chemistry and Physics Discussions

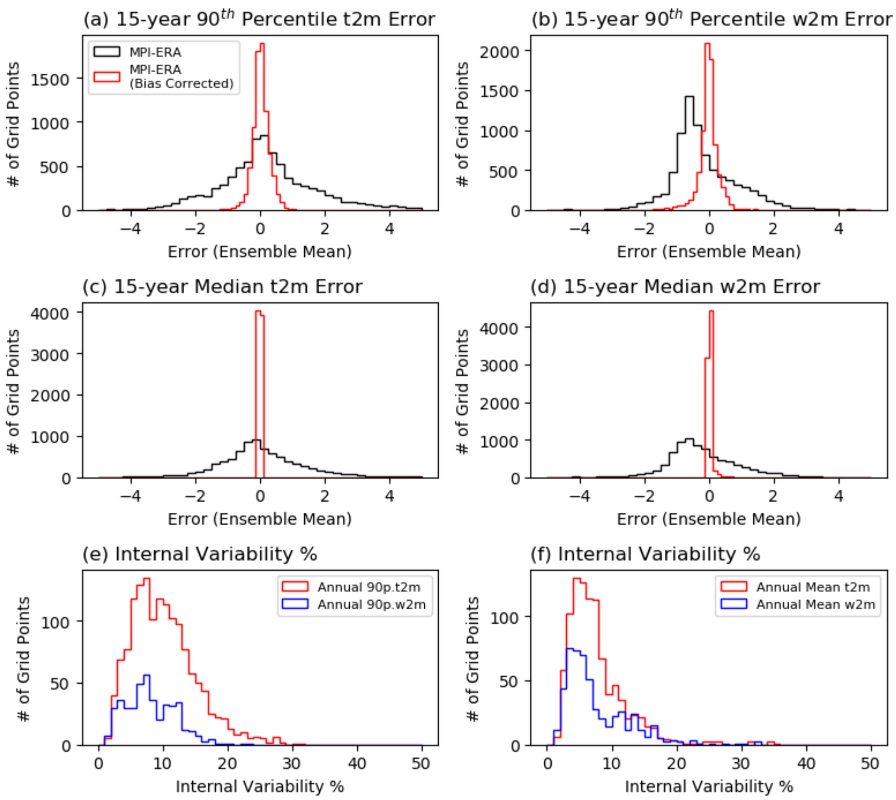

Figure 2. Histogram of (a, c) 2m temperature and (b, d) wet bulb temperature error (MPI minus ERA) between ERA-Interim and 1% MPI runs with the same global average temperature. The error of the (a, b) 15-year 90th percentile and (c, d) median are shown. (e, f) The percentage of unforced variability (maximum ensemble member – minimum ensemble member) against absolute value of the average difference with reanalysis.

https://doi.org/10.5194/acp-2021-109
Preprint. Discussion started: 22 February 2021

Atmospheric Chemistry and Physics
Discussions
Open Access
EGU

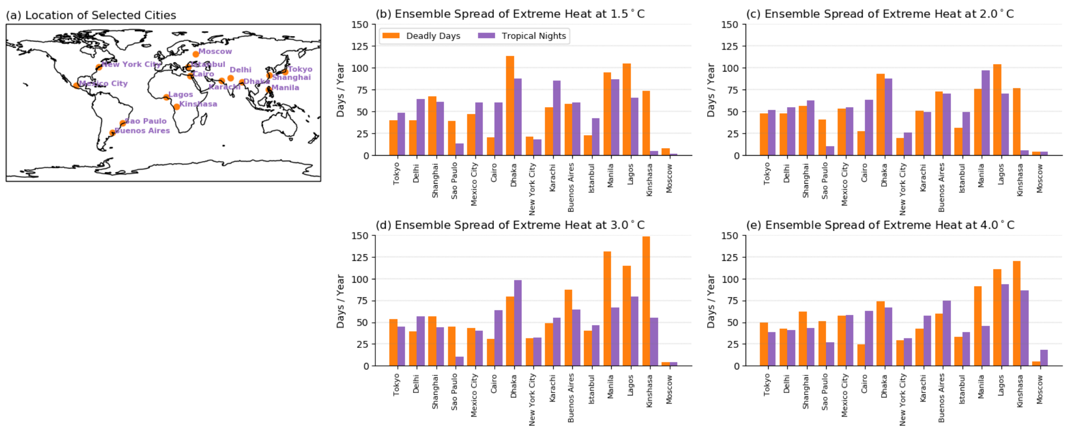

Figure 3. (a) Location of 15 selected cities and spread of heat extremes between ensemble members in (b) 1.5, (c) 2.0, (d) 3.0, and (e) 4.0°C of global warming. Ensemble with smallest heat extreme days are deducted from the ensemble with most heat extreme days to calculate the spread. Number of heat extreme days are calculated by averaging 3×3 grid covering the selected city.

https://doi.org/10.5194/acp-2021-109
Preprint. Discussion started: 22 February 2021

Atmospheric Chemistry and Physics Discussions
Open Access

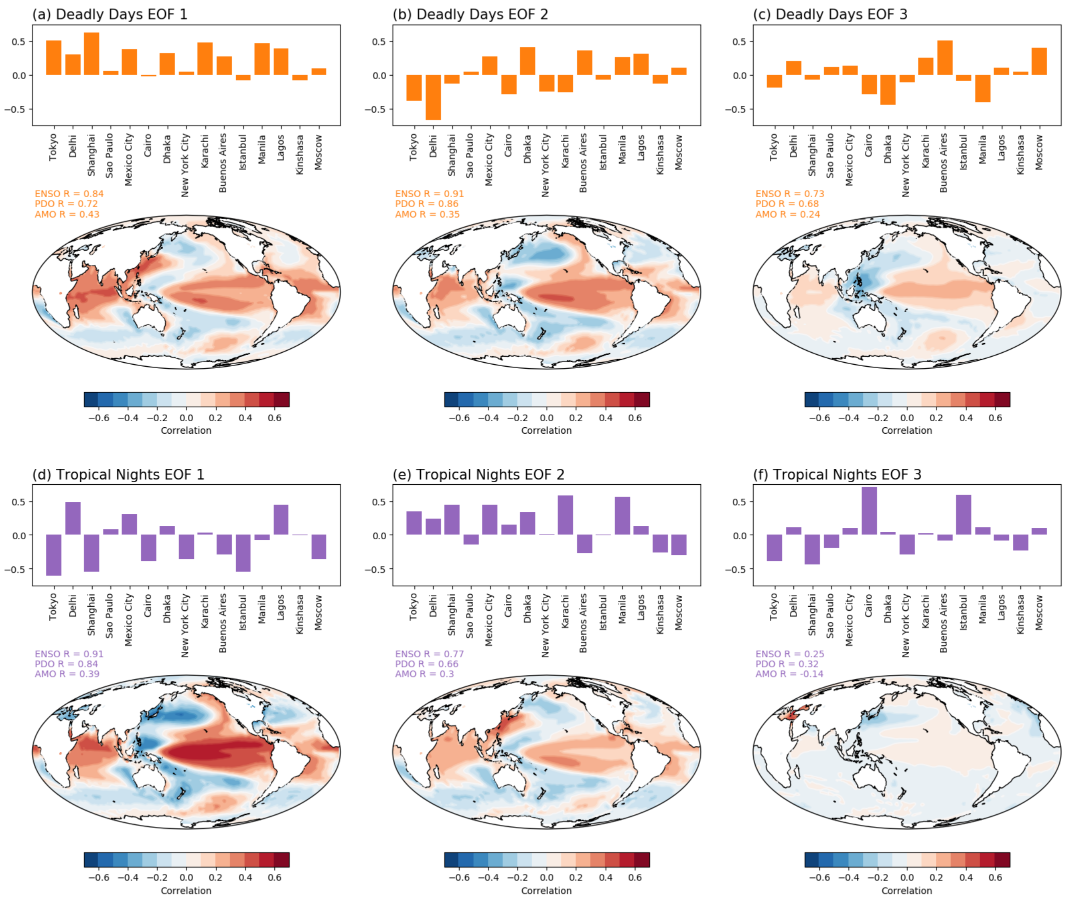

Figure 4. First three EOFs of deadly days (a, b, c) and tropical nights (d, e, f) in 15 cities. Heat extremes in 15 cities are linearly detrended and normalized before EOF analysis. For each panel, the bar graph shows the EOF pattern of the number of heat extremes days per year. Contour plots shows the SST pattern associated with the EOF mode, obtained by projecting each mode of PC onto SST anomalies. Ensemble members are averaged to yield the SST pattern. Pattern correlation with major modes of climate variability (ENSO, PDO, AMO) are also shown, as discussed in the text.

https://doi.org/10.5194/acp-2021-109
Preprint. Discussion started: 22 February 2021

Atmospheric Chemistry and Physics Discussions
Open Access

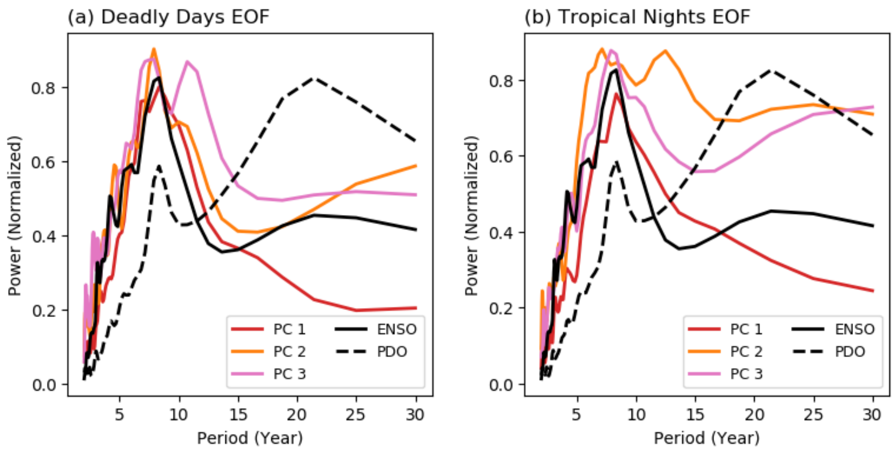

Figure 5. Frequency power spectrum of ENSO, PDO, and PC of first three EOF modes for (a) deadly days and (b) tropical nights. ENSO is calculated with the Niño 3.4 Index, and PDO is calculated as a leading EOF of SST anomaly in North Pacific basin. Monthly SST data is used for both ENSO and PDO, and then each index is averaged over the year to have consistency with deadly days and tropical nights.

https://doi.org/10.5194/acp-2021-109
Preprint. Discussion started: 22 February 2021

Atmospheric Chemistry and Physics Discussions

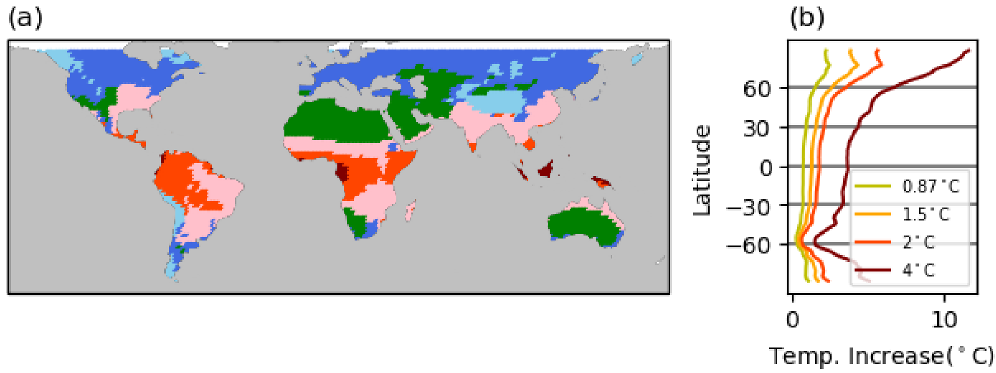

Figure 6. (a) Clustered regions via K-means clustering. (b) Zonal average of temperature increases at the time of 0.87°C (current climate), 1.5°C, 2°C, and 4°C of global warming compared to pre-industrial baseline in the 1% runs. Temperatures are averaged over a 5-year period after each warming threshold is observed.

https://doi.org/10.5194/acp-2021-109
Preprint. Discussion started: 22 February 2021

Atmospheric Chemistry and Physics Discussions
Open Access

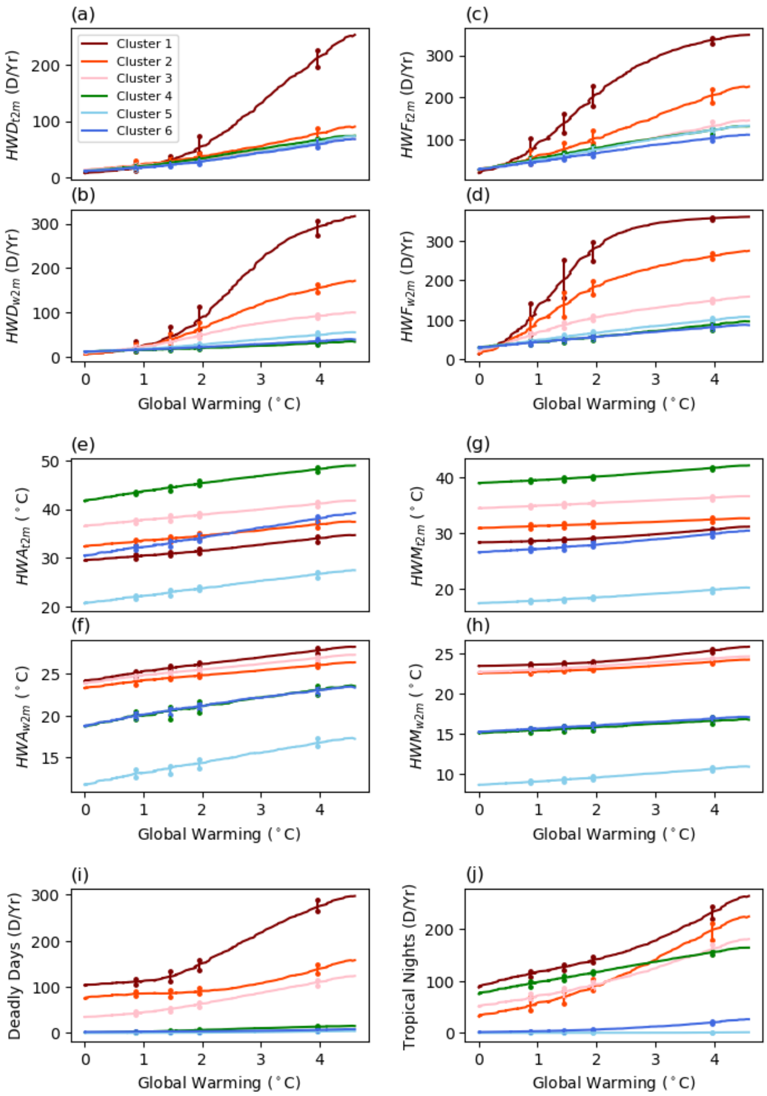

Figure 7. Evolution of each index averaged over each cluster. Values of each metric are calculated by averaging grid points belonging to each cluster separately for each ensemble. Vertical lines with dots show the maximum and minimum of 28 ensemble members at each threshold of warming to represent the spread between the ensemble.

https://doi.org/10.5194/acp-2021-109
Preprint. Discussion started: 22 February 2021

Atmospheric Chemistry and Physics Discussions

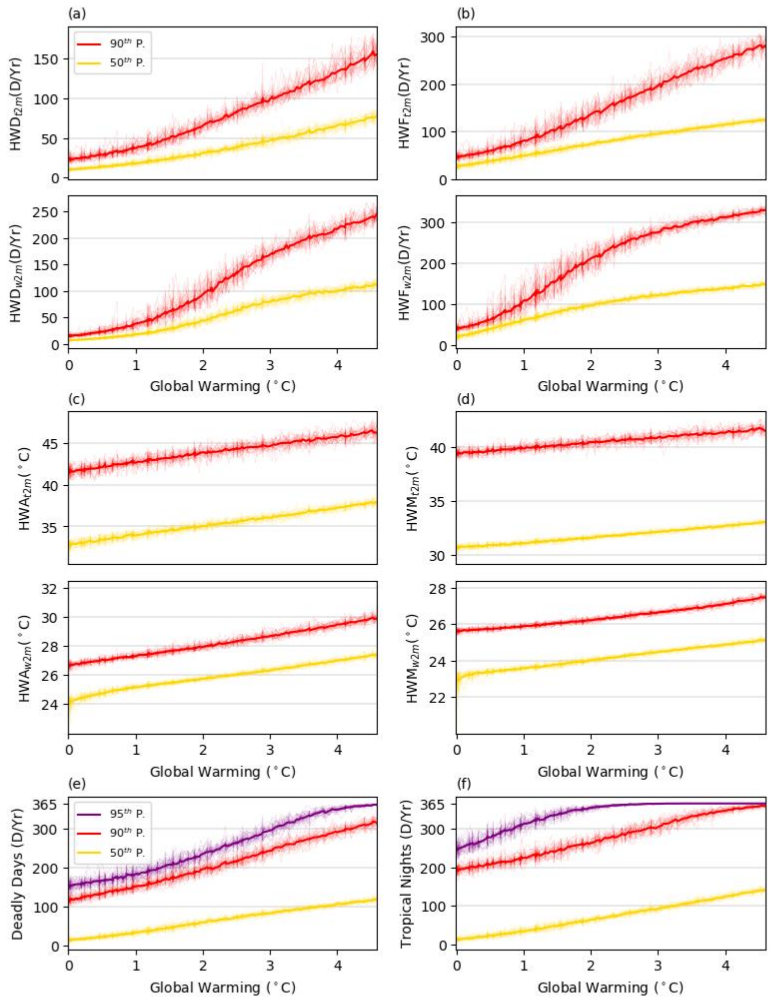

Figure 8. Changes of population-weighted heat wave indices at each level of global warming. Each line denotes one ensemble member for percentile of population.

https://doi.org/10.5194/acp-2021-109
Preprint. Discussion started: 22 February 2021

Atmospheric Chemistry and Physics Discussions

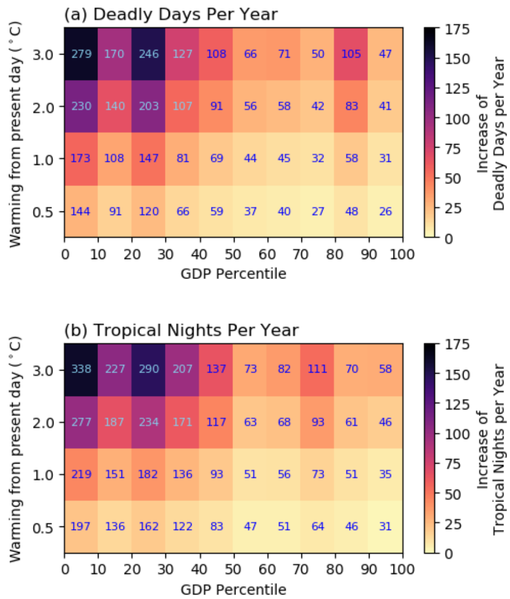

Figure 9. Increase in (a) Deadly Days and (b) Tropical Nights compared to our present climate, binned by percentile of GDP per capita at selected levels of warming compared to present day, averaged over the population within the GDP percentile (for example, averaged over population in 0~10 percentile of GDP), and over all ensemble members for 5-year window after each level of warming first occurs. Blue text inside the heatmap represent the absolute of Deadly Days and Tropical Nights in each level of warming above present day.

https://doi.org/10.5194/acp-2021-109
Preprint. Discussion started: 22 February 2021

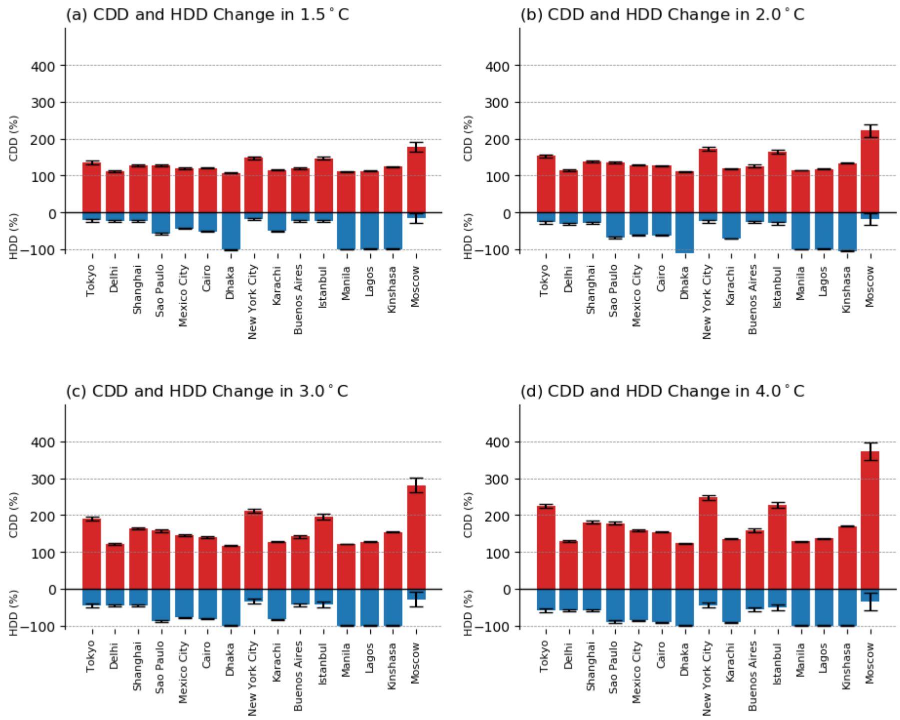

Figure 10. CDD (red bar) and HDD (blue bar) values at each levels of global warming, divided by the pre-industrial CDD and HDD for 15 selected cities. Error bars show the standard deviation between the ensemble members.

https://doi.org/10.5194/acp-2021-109
Preprint. Discussion started: 22 February 2021

Atmospheric Chemistry and Physics Discussions

Table 1. Explanation of heat wave indices used in this study.

Acronym	Index	Definition	Units
$HWD_{t2m/w2m}$	Heat wave duration	Length of longest period of consecutive heat wave days in a year	# days
$HWF_{t2m/w2m}$	Heat wave frequency	Total number of heat wave days in a year	# days
$HWA_{t2m/w2m}$	Heat wave amplitude	Maximum temperature over all heat wave days in a year	°C
$HWM_{t2m/w2m}$	Heat wave mean	Average temperature over all heat wave days in a year	°C
Deadly Days	Deadly Days	Daily maximum wet-bulb temperature over 24°C	# days
Tropical Nights	Tropical Nights	Daily minimum temperature over 25°C	# days
CDD	Cooling degree days	Sum of positive values after removing 18°C from daily average temperature	°C days
HDD	Heating degree days	Absolute value of sum of negative values after removing 18°C from daily average temperature	°C days

https://doi.org/10.5194/acp-2021-109
Preprint. Discussion started: 22 February 2021

Atmospheric Chemistry and Physics Discussions

Table 2. Percentage area and major regions belonging to each cluster. Clusters are identified only for the global land areas.

Cluster	Color	Area percentage (%)	Major regions	Cluster name
1	Maroon	2.95	Indonesia, Malaysia, Cameroon, Gabon	Tropical West Pacific
2	Orange	12.34	Northern South America, Central Africa	Tropical Africa and America
3	Pink	22.70	India, Southeast Asia, Eastern South America, Southeast U.S.	Sub-Tropical Asia and America
4	Green	21.55	Northern Africa, Middle East, Australia	Deserts
5	Sky blue	7.69	Himalayas, Andes	Mountain Range
6	Blue	32.75	Canada, Northwest U.S., Russia	Sub-Polar Region

https://doi.org/10.5194/acp-2021-109
Preprint. Discussion started: 22 February 2021

Table 3. Number of deadly days each percentile of global population faces with 0.87°C (current period), 1.5°C, 2°C, 3°C, and 4°C global warming from the pre-industrial condition. Standard deviations between the ensembles (1σ) are also shown.

		Global Warming				
	Population	0.87°C	1.5°C	2.0°C	3.0°C	4.0°C
Deadly Days	95th p.	180 (± 13)	204 (± 14)	228 (± 15)	297 (± 15)	349 (± 6)
	90th p.	148 (± 8)	170 (± 9)	190 (± 13)	244 (± 11)	292 (± 10)
	50th p.	31 (± 3)	44 (± 6)	58 (± 5)	84 (± 4)	105 (± 4)
Tropical Nights	95th p.	302 (± 14)	333 (± 9)	350 (± 4)	364 (± 1)	365 (± 0)
	90th p.	217 (± 9)	241 (± 13)	262 (± 10)	306 (± 16)	345 (± 7)
	50th p.	32 (± 5)	47 (± 7)	61 (± 5)	94 (± 6)	122 (± 5)